forum acusticum 2026
8-12 September · Graz, Austria

Numerical evidence of multiple scattering of photoacoustic waves in blood

Ujjal Mandal[1], Navroop Singh[2], Kartikay Singh[2], Vinit Nana Hagone[2], Jagpreet Singh[2], Anshu S Anand[3], Ben T Cox[4], Ratan K Saha[1]

[1]*Department of Applied Sciences, Indian Institute of Information Technology Allahabad, Jhalwa, Prayagraj 211015, Uttar Pradesh, India*
[2]*Department of Computer Science and Engineering, Indian Institute of Technology Ropar, Street 29, Ropar, 140001, Punjab, India*
[3]*Department of Information Technology, Indian Institute of Information Technology Allahabad, Jhalwa, Prayagraj 211015, Uttar Pradesh, India*
[4]*Department of Medical Physics and Biomedical Engineering, University College London, Gower Street, London, WC1E 6BT, UK*

This paper is a revised version of the authors' submitted manuscript that was peer-reviewed by at least two anonymous reviewers.

Abstract

Overall photoacoustic (PA) wave field in blood is strongly influenced by acoustic scattering arising from spatial distribution and acoustic properties of red blood cells (RBCs). In this study, the effect of multiple scattering of acoustic waves in blood with 30% hematocrit is numerically investigated using the convergent Born series (CBS) method. The simulation result is compared with that of a discrete particle approach (DPA). While the DPA estimates the total pressure field as a linear superposition of fields emitted by individual particles, it neglects the contribution owing to the multiple scattering of acoustic waves. The CBS method incorporates wave-cell interactions through an iterative Born series procedure. Simulations were performed for an ensemble of RBCs randomly distributed in a computational domain of size 2048×2048 grid points, and the pressure fields were calculated at 88 MHz for three different acoustic impedance mismatch conditions. The CBS technique can exhibit modification of the pressure field occurring due to multiple scattering of PA waves in blood.

Keywords: *Photoacoustics, RBCs, Blood, Scattering, Discrete particle approach (DPA), Born series, Central processing unit (CPU), Graphics processing unit (GPU), Parallel computation*

***Corresponding author**: ratank.saha@iiita.ac.in.*

1. Introduction

The photoacoustic (PA) imaging has emerged as a powerful biomedical modality for investigating optical absorption properties of biological tissues [1]. Various PA tomography and microscopy technologies have been developed to achieve the same. Blood is a strong absorber of light energy and hence generates PA signals when illuminated with short laser pulses. In particular, chemical states and the abundance of red blood cells (RBCs) dictate how much light energy will be absorbed by blood. It may be mentioned here that the PA technique can quantify blood parameters such as hemoglobin concentration and oxygen saturation [1], [2].

The numerical methods for solving the time-dependent PA wave equation reflect the need for improved accuracy and computational efficiency. One popular method to solve the time-dependent PA wave equation is the Finite Difference Time Domain (FDTD) scheme. It was initially used due to its simplicity, but requires dense grids, leading to high computational cost, especially at high frequencies [3], [4]. To reduce numerical dispersion and improve efficiency, the k-Wave pseudospectral method was introduced [5], which uses spectral techniques to accomplish better accuracy with fewer grid points.

However, the time-domain approaches remain expensive for large or steady state problems, and thus the Finite Difference Frequency Domain (FDFD) method was tried as well [6]. The traditional Born series (TBS) technique is a frequency domain and an iterative method to solve the time-independent wave equation (i.e., the inhomogeneous Helmholtz equation). It is a computationally efficient approach, works well

for regular and irregular source geometries, but is limited to weak scattering problems only [7]. To overcome this limitation, the convergent Born series (CBS) was developed, enabling stable and accurate solutions even in strongly inhomogeneous media with multiple scattering effects.

In this work, we apply the CBS method to estimate the PA field generated by a numerical blood sample consisting of acoustically inhomogeneous RBCs and the same has been compared with that of an analytical method that assumes independent scattering. The present study may be relevant to high frequency PA microscopy and blood characterization where acoustic interaction among closely packed erythrocytes may influence the detected PA signals.

2. Methodology

2.1. Discrete particle approach (DPA)

Consider that a 2D region is occupied by N number of disks mimicking acoustically inhomogeneous RBCs. The PA field for a collection of such particles may be written as [8],

$$\psi_{DPA}(\mathbf{r}) = A\sum_{n=1}^{N} B_n, \tag{1}$$

where $B_n = \frac{J_1(k_s a_n)H_0^1(k_f|\mathbf{r}-\mathbf{r}_n|)}{k_s[J_1(k_s a_n)H_0^1(k_f a_n)-\hat{\rho}\hat{v}J_0(k_s a_n)H_1^1(k_f a_n)]}$. Here, $\mathbf{r}$ is the position vector of the field point (it is outside of any source), and the same quantity for the nth source is $\mathbf{r_n}$ with radius a_n. And, k_s and k_f denote the wave numbers of the source region and the ambient medium, respectively; the subscripts s and f represent the source and the surrounding fluid media, respectively; $\hat{\rho} = \rho_s/\rho_f$ and $\hat{v} = v_s/v_f$; ρ and v being the density and speed of sound, respectively. Further, $A = i\mu\beta I_0 v_s/C_p$, with ω and I_0 being the modulation frequency and intensity of the incident light beam, respectively; μ, β, and C_P indicate the optical absorption coefficient, isobaric thermal expansion coefficient, and specific heat for the absorbing region, respectively. The notations J and H^1 represent the Bessel function and the Hankel function of the first kind, respectively. The subscripts 0 and 1 indicate the orders of each function. In Eq. (1), the total field is obtained by using the linear superposition principle, and thus the issue of multiple scattering of waves due to acoustically inhomogeneous PA sources has been ignored.

2.2. Born series

For the PA pressure $\psi(\mathbf{r})$ at point $\mathbf{r}$ with source term $S(\mathbf{r})$ and the scattering potential $V(\mathbf{r}) = k_s^2 - k_f^2 - i\epsilon$ where ϵ is a positive real number [7], [8], [9], with background wave number k_f and constant density, the inhomogeneous Helmholtz equation can be written as [8],

$$\nabla^2\psi(\mathbf{r}) + (k_f^2 + i\epsilon)\psi(\mathbf{r}) = -S(\mathbf{r}) - V(\mathbf{r})\psi(\mathbf{r}), \tag{2}$$

$$S(\mathbf{r}) = \begin{cases} -\frac{i\mu\beta I_0\omega}{C_p}, & \text{if } |\mathbf{r}| \le a_n \\ 0, & \text{if } |\mathbf{r}| > a_n \end{cases} \tag{3}$$

and,

$$V(\mathbf{r}) = \begin{cases} k_s^2 - k_f^2 - i\epsilon, & \text{if } |\mathbf{r}| \le a_n \\ -i\epsilon, & \text{if } |\mathbf{r}| > a_n \end{cases} \tag{4}$$

with $n \in 1, \ldots, N$. The integral formulation of Eq. (2) is given by [7], [8],

$$\psi(\mathbf{r}) = \int g(\mathbf{r}|\mathbf{r}_0)[V(\mathbf{r}_0)\psi(\mathbf{r}_0) + S(\mathbf{r}_0)]d^2\mathbf{r}_0, \tag{5}$$

where, the integration is over the entire space $\mathbb{R}^2$ (as we are dealing with a 2D problem) and $g(\mathbf{r}|\mathbf{r}_0)$ is the Green's function that satisfies the following equation [7], [8], [10],

$$\nabla^2 g(\mathbf{r}|\mathbf{r}_0) + (k_f^2 + i\epsilon)g(\mathbf{r}|\mathbf{r}_0) = -\delta(\mathbf{r} - \mathbf{r}_0), \tag{6}$$

here, $\delta(\mathbf{r} - \mathbf{r}_0)$ is the Dirac delta function; Eq. (5) involves convolution sums and hence, can be cast as [7], [8],

$$\psi = GV\psi + GS, \tag{7}$$

where $G = \mathcal{F}^{-1}\tilde{g}(\mathbf{p})\mathcal{F}$; the symbols $\mathcal{F}$ and $\mathcal{F}^{-1}$ refer to the forward and inverse Fourier transform operators, respectively; $\tilde{g}(\mathbf{p})$ is the Fourier transform of $g(\mathbf{r}|\mathbf{r}_0)$ and is given by [7], [8],

$$\tilde{g}(\mathbf{p}) = \frac{1}{(|\mathbf{p}|^2 - k_f^2 - i\epsilon)}, \tag{8}$$

with $|\mathbf{p}|$ is the Fourier transformed coordinates.

2.3. Convergent Born series (CBS)

Let Eq. (7) is multiplied by a preconditioner $\mho$ facilitating [7],

$$\mho\psi = \mho GV\psi + \mho GS. \tag{9}$$

Eq. (9) can be rewritten as [7],

$$\psi = M\psi + \mho GS, \tag{10}$$

where $M = \mho GV - \mho + 1$ and recursive expansion of Eq. (10) provides an infinite series as,

$$\psi = \sum_{n=0}^{\infty} M^n \mho GS, \tag{11}$$

The spectral norm should be $|M| < 1$ for the convergence of the above series. Additionally, it can be proved that the above series converges for all structures if $\mho = \frac{i}{\epsilon}V(\mathbf{r})$ and $\epsilon \ge \max(|k_s^2 - k_f^2|)$ [7], [11].

2.4. Computational implementation

Eq. (11) has been realized in this study to compute the pressure fields at different frequencies. The corresponding infinite sum can be accomplished iteratively

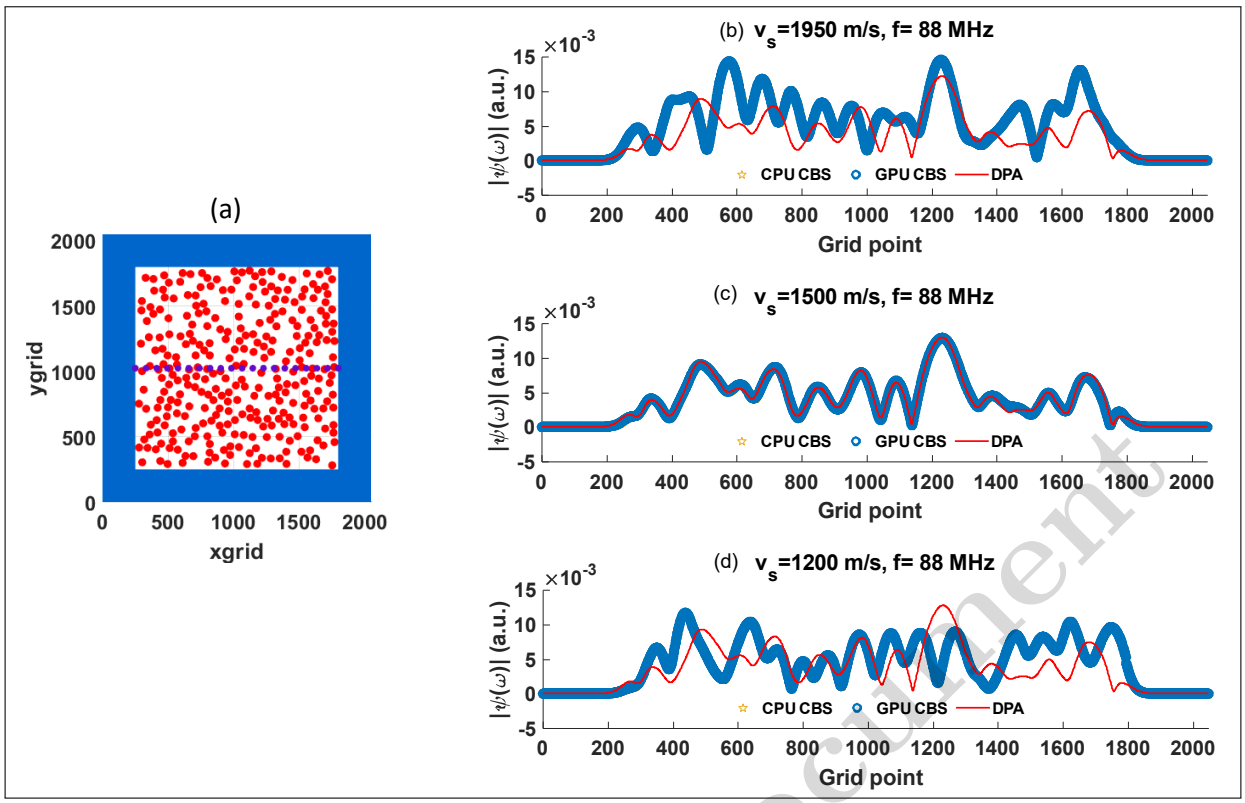

Figure 1: (a) Demonstration of a simulated tissue configuration. A total of 302 solid circular disks (resembling RBCs) are randomly distributed within the white, which is enclosed by the blue strips (ABL). RBCs occupy 30% area of the white region. The location of the RBCs was generated using the well-known Metropolis-Hastings algorithm. The PA pressure data are recorded along the center line (filled violet dots). (b) Plots of PA pressure computed at 88 MHz generated by the tissue realization through the center line at different sound speed contrasts; v_s=1950, 1500, 1200 m/s for (b), (c), (d), respectively, with three implementations: CPU CBS, GPU CBS, and DPA.

as,

$$\psi_{CBS_{l+1}}(\mathbf{r}) = \psi_{CBS_l}(\mathbf{r}) - \mho\left(\psi_{CBS_l}(\mathbf{r}) - \mathcal{F}^{-1}[\tilde{g}(\mathbf{p})\mathcal{F}[V(\mathbf{r})\psi_{CBS_l}(\mathbf{r}) + S(\mathbf{r})]]\right), \tag{12}$$

where the field at the 0th iteration is given by,

$$\psi_{CBS_0}(\mathbf{r}) = \mho\mathcal{F}^{-1}[\tilde{g}(\mathbf{p})\mathcal{F}S(\mathbf{r})]). \tag{13}$$

Further, all the multiplications have to be performed element-wise.

3. Simulation experiment

A two-dimensional computational domain (2048 × 2048) was discretized using uniform grids ($dx = dy$ = 100 nm) and created to model a tissue realization composed of randomly distributed RBCs. Each RBC was modeled as a circular disk. The spatial distribution of the disks was generated using the Metropolis-Hastings algorithm to ensure a non-overlapping configuration. In the present study, the cells occupied approximately 30% area fraction within the region of interest as per Fig. 1 (a). The density was chosen to be $\rho_s = \rho_f = 1000$ kg/m^3. The speed of sound for the surrounding medium was fixed to $v_f = 1500$ m/s, and the sound-speed inside the source was chosen as $v_s = 1950$, 1500, and 1200 m/s. These values were selected to generate positive, zero, and negative sound-speed contrast conditions, respectively with respect to the surrounding medium ($v_f = 1500$ m/s). The case $v_s = 1500$ m/s corresponds to an acoustically homogeneous medium where scattering effects are absent, but $v_s = 1950$ m/s and 1200 m/s represent positive (+30%) and negative (-20%) sound-speed contrasts. These values were chosen to investigate how the magnitude and nature of acoustic contrast influence multiple scattering effects and the resulting PA pressure field.

The PA field was calculated at 88 MHz. The numerical values of optical, mechanical, and thermodynamical parameters were set to be unity ($I_0 = 1$, $\mu = 1$, $\beta = 1$, $C_p = 1$). The absorbing boundary layer (ABL) was incorporated at edges using the sigmoid function, which ensured a non-reflection condition for the outgoing waves and also did not reappear from the opposite boundary [8], [12]. It is defined as,

$$ABLFn(x) = \frac{1}{1 + e^{-\kappa(x-0.5d)}}, \text{within the ABL} \tag{14}$$

where $x > 0$ and d is the thickness of the ABL ($d = 500$ grid points); $\kappa = 61.36 \times 10^2$ np/cm; otherwise it was

taken as $ABLFn(x) = 1.0$. The final pressure field was updated as $\psi_{l+1} = ABLFn \times \psi_{l+1}$. The total error for the center line was calculated and it was defined as,

$$\text{Error} = \frac{\sum_{m=1}^{2048} |\psi_{l+1}(1024, m) - \psi_l(1024, m)|}{\sum_{m=1}^{2048} |\psi_l(1024, m)|}. \tag{15}$$

The system reached its steady state if the error was less than 0.0001 [8], [12], [13]. A C code (running in a CPU machine) and a CUDA C code (running in a GPU machine) were written to realize Eq. (12). The corresponding results are referred to as CPU CBS and GPU CBS, respectively in the remaining text.

4. Simulation results and discussion

The magnitude of PA pressure (carrier wave) along the x-axis (center line of the computational domain) for a tissue realization at 88 MHz is shown in Fig. 1(b) when the sound-speed contrast is 30%. The same plots for other cases are displayed in 1(c) and (d), respectively. Simulation results for three different approaches, namely, CPU CBS, GPU CBS and DPA are included in each figure. All the methods produce the same result when the sound-speed mismatch is nil; however, noticeable differences between the CBS and DPA techniques are observed when sound-speed contrast exists between the cells and the surrounding medium. The CBS simulations capture the effect of multiple scattering of acoustic waves occurring due to the inhomogeneous nature of the scatterers. This aspect is absent in the DPA model, which sums up the contributions of PA pressure emitted by individual cells. The computationally intensive loops in the CPU code were parallelized using the industry-standard Open Multi-Processing application programming interface. The GPU-based implementation significantly reduced the execution time compared to CPU computation. For instance, for a particular contrast and frequency, CPU runtime was 14 s, while that of the GPU was about 1.5 s on a workstation [8], [12].

It may be pointed out that the probing frequency was fixed at 88 MHz because higher frequencies provide wavelengths that are more comparable to erythrocyte dimensions, thereby enhancing wave-cell interactions and making multiple-scattering effects more observable. In contrast, at the lower frequency range typically employed in PA tomography (1–20 MHz), the acoustic wavelength is much larger than the dimensions of the individual erythrocytes, and hence, the influence of scattering is expected to be less pronounced. Therefore, 88 MHz was chosen as a representative frequency for studying the underlying physical mechanisms and demonstrating the capability of the CBS framework to capture multiple-scattering effects in blood.

Although blood is known to exhibit significant echogenicity in ultrasound and the Doppler imaging [14], the impact of multiple scattering of photoacoustically generated acoustic waves within blood has not been investigated yet as far as we know. Since erythrocytes act as both optical absorbers and acoustically inhomogeneous sources, interactions among neighboring cells may modify the resulting PA field and influence quantitative PA measurements.

A possible experimental validation may involve a blood sample, intensity modulated optical excitation and a high frequency US detector positioned close to the sample. It should make a raster scan to collect position-dependent signals. Such signals have to be Fourier transformed to obtain frequency dependent information. A detector with sufficient bandwidth and high signal to noise ratio would facilitate the observation of multiple scattering effects predicted by the present numerical framework.

5. Conclusions

The CBS technique has been found to be a reliable and flexible method for handling complex systems involving multiple scatterers. It effectively captures interactions between acoustically inhomogeneous sources, including multiple scattering effects that significantly influence the internal pressure distribution, especially in heterogeneous tissues. This framework provides valuable information on PA field formation and propagation. The CBS calculations can suitably be implemented in a GPU architecture, enabling very fast estimation of the pressure field. It establishes a strong foundation for future experimental validation, which may contribute to improved PA microscopy imaging and more accurate tissue characterization.

6. Acknowledgments

The Central Computing Facility at the Indian Institute of Information Technology, Allahabad, is acknowledged, where simulations were executed. UM thanks the members of the Biomedical Imaging Laboratory (BMIL) for continuous support and UGC-NFSC (Grant No. #F. 82-44/2020 (SA-III)) for providing a stipend. RKS acknowledges the financial support received from ANRF (#CRG/2023/003278). BTC thanks EPSRC, UK, grants EP/W029324/1 and EP/T014369/1.

References

[1] J. J. M. Riksen, A. V. Nikolaev, and G. van, "Photoacoustic imaging on its way toward clinical utility: A tutorial review focusing on practical application in medicine," *Journal of Biomedical Optics*, vol. 28, no. 12, p. 121 205, 2023.

[2] S. Paul, H. S. Patel, V. Misra, R. Rani, A. K. Sahoo, and R. K. Saha, "Numerical and in vitro experimental studies for assessing the blood hematocrit and oxygenation with the dual-wavelength photoacoustics," *Photoacoustics*, vol. 39, p. 100 642, 2024.

[3] A. Taflove and S. C. Hagness, *Computational Electrodynamics: The Finite-Difference Time-Domain Method*. Artech House, 2005.

[4] Y. L. Sheu and P. C. Li, "Simulations of photoacoustic wave propagation using a finite-difference time-domain method with berenger's perfectly matched layers," *The Journal of the Acoustical Society of America*, vol. 124, no. 6, pp. 3471–3480, 2008.

[5] B. E. Treeby and B. T. Cox, "K-wave: Matlab toolbox for the simulation and reconstruction of photoacoustic wave fields," *Journal of Biomedical Optics*, vol. 15, no. 2, p. 021 314, 2010.

[6] R. M. Moreira et al., "Frequency-domain acoustic-wave modeling with hybrid absorbing boundary conditions," *Geophysics*, vol. 79, no. 3, T105–T116, 2014.

[7] M. Osnabrugge, S. Leedumrongwatthanakun, and I. M. Vellekoop, "A convergent born series for solving the inhomogeneous helmholtz equation in arbitrarily large media," *Journal of Computational Physics*, vol. 322, pp. 113–124, 2016.

[8] U. Mandal et al., "Efficient implementations of a born series for computing photoacoustic field from a collection of erythrocytes," *Photoacoustics*, vol. 43, p. 100 724, 2025.

[9] A. Kaushik, P. Yalavarthy, and R. K. Saha, "Convergent born series improves the accuracy of numerical solution of time-independent photoacoustic wave equation," *Journal of Modern Optics*, vol. 67, no. 9, pp. 849–855, 2020.

[10] R. K. Saha, "Solving time-independent inhomogeneous optoacoustic wave equation numerically with a modified green's function approach," *Journal of the Acoustical Society of America*, vol. 149, no. 6, pp. 4039–4048, 2021. DOI: 10.1121/10.0005973.

[11] R. K. Saha, "Numerical solution to the time-independent inhomogeneous photoacoustic wave equation using the born series methods," *Journal of the Optical Society of America A*, vol. 37, no. 12, pp. 1907–1915, 2020. DOI: 10.1364/JOSAA.401398.

[12] U. Mandal, J. Singh, B. T. Cox, and R. K. Saha, "Graphics processing unit accelerated helmholtz equation solver in two dimensions using the traditional born series formulation for linear and nonlinear media in biomedical ultrasound," *The Journal of the Acoustical Society of America*, vol. 159, no. 3, pp. 1948–1962, Mar. 2026.

[13] U. Mandal, J. Singh, and R. K. Saha, "On the born series methods for solving inhomogeneous helmholtz equation in biomedical photoacoustics," in *Opto-Acoustic Methods and Applications in Biophotonics VI*, ser. Proc. SPIE, vol. 12631, 2023, 126310W.

[14] P. Dong-Guk, L. Cheong-Ah, and I. Cynthia, "Principles of doppler ultrasound and emerging blood flow imaging," *Ultrasonography*, vol. 44, no. 6, pp. 409–424, 2025.